Three-Coordinate Zinc Methyl Complexes with Sterically Demanding Formazanate Ligands

de Vries, Folkert; Travieso-Puente, Raquel; Roewen, Peter; Otten, Edwin

Published in:
Organometallics

DOI:
10.1021/acs.organomet.0c00720

ORGANOMETALLICS

pubs.acs.org/Organometallics

Article

Three-Coordinate Zinc Methyl Complexes with Sterically Demanding Formazanate Ligands

Folkert de Vries, Raquel Travieso-Puente, Peter Roewen, and Edwin Otten*

Cite This: *Organometallics* 2021, 40, 63−71

Read Online

ACCESS | Metrics & More | Article Recommendations | Supporting Information

ABSTRACT: A series of heteroleptic three-coordinate mono(formazanate)zinc methyl complexes were synthesized, and the influence of the ligand on the structure as well as redox and optical properties of these complexes was investigated. The heteroleptic mono(formazanate)zinc methyl complexes were found to show ligand redistribution in solution, reminiscent of the Schlenk equilibrium, to generate an equilibrium mixture containing the corresponding homoleptic complexes as well. Monitoring the approach to equilibrium by NMR spectroscopy in benzene-d_6 allowed determination of the forward and backward rate constants. A correlation was found between the steric environment around the zinc center and equilibrium concentration of (formazanate)-zinc methyl compounds, whereas the kinetics for approach to equilibrium are also dependent on the electronic properties.

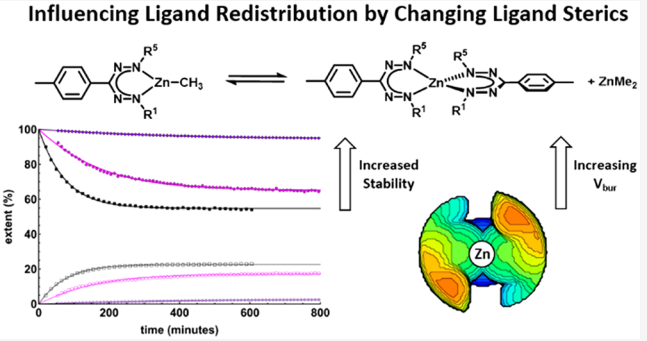

INTRODUCTION

Ligand design is key to the development of new structures and reactivity in organometallic chemistry. In particular, sterically demanding ligands have been instrumental in providing access to highly reactive, low-coordinate complexes that are relevant for catalysis. An illustration of this is provided by the 2013−2014 *Organometallics* Roundtable, where (bulky) ligand synthesis was identified as a major challenge for the field.[1] β-Diketiminate (BDI) ligands are a case in point. Despite being used as ligands since the 1960s,[2] their popularity in organometallic chemistry was boosted during the mid-1990s with the discovery of sterically demanding versions of the β-diketiminate ligand.[3] This has made it possible to obtain monomeric, low-coordinate organometallic complexes, enabling the study of highly reactive species such as monomeric metal hydrides[4] and unusual low-valent Mg compounds.[5] Moreover, these ligands have provided well-defined species that can be applied in homogeneous catalysis,[6] such as hydroamination,[7] hydrophosphination,[8] and hydrosilylation,[9] among others. In particular, three-coordinate zinc complexes bearing BDI ligands have shown great promise in a variety of polymerization reactions, such as ring-opening polymerization (ROP) of lactide[10] or the copolymerization of CO_2 with epoxides.[11]

The popularity of β-diketiminate ligands in part originates from their modular synthesis, which provides facile access to a large variety of different substitution patterns. This includes ligands with sterically demanding N-substituents exemplified by the often-used 2,6-diisopropylphenyl group (DIPP, **A**, Chart 1), which effectively protects the metal complex from deleterious reactions (ligand redistribution and other decomposition pathways). Sterically demanding dipyrrinato ligands (**B**, Chart 1) were introduced in the past decade by Betley and co-workers to access low-coordinate complexes with first-row transition metals, resulting in unusual terminal imidos that are active in C−H bond amination.[12] Moreover, these ligands were recently also used by Harder and co-workers to obtain monomeric zinc hydride complexes.[13]

Chart 1. Representative "Bulky" Bidentate N-Donor Ligands

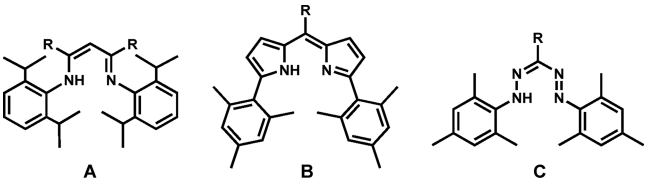

Our group has in recent years developed the coordination chemistry of formazanate ligands (**C**, Chart 1) as analogues of β-diketiminates. Although the two ligand structures are similar, the exchange of two carbon atoms in the β-diketiminate NCCCN ligand backbone for nitrogen (i.e., NNCNN) makes

Received: November 12, 2020
Published: December 23, 2020

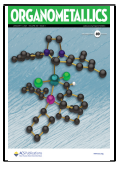

https://dx.doi.org/10.1021/acs.organomet.0c00720
Organometallics 2021, 40, 63−71

Scheme 1. General Synthetic Routes toward Triaryl Formazans

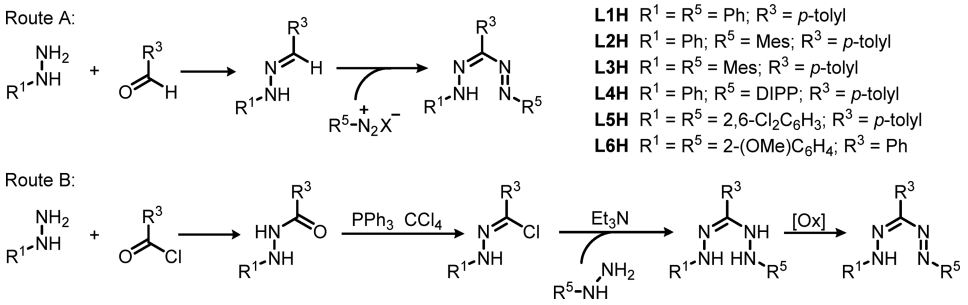

that formazanate ligands have low-lying π^*-orbitals and thus are redox-active.[14] Following our initial report on homoleptic bis(formazanate)zinc complexes, which were isolated in three distinct redox-states arising from ligand-based reduction,[15] we and others have started a systematic investigation of formazanate coordination compounds with both main group elements and transition metals.[16] Despite significant advances in this field in the past decade, it has proven challenging to prepare triaryl formazanate ligands with a steric profile sufficient to stabilize low-coordinate formazanate complexes and study their (catalytic) reactivity. Indeed, attempts to prepare low-coordinate mono(formazanate) metal complexes with simple, unhindered ligands results instead in formation of bis(formazanate) complexes as the thermodynamic products via ligand redistribution.[17]

In this work we present a series of heteroleptic three-coordinate (formazanate)zinc methyl complexes and their ligand redistribution reactions to form the corresponding homoleptic compounds. Monitoring the approach to equilibrium allows determination of the thermodynamic stability of the heteroleptic complexes, which is dependent on the size of the N−Ar substituents. In addition, the rates of ligand exchange are sensitive to the electronic properties of the ligand (electron-donating ability).

RESULTS AND DISCUSSION

Ligand Synthesis. Formazan ligands **L1H**−**L3H**[18] were synthesized by using literature procedures, involving the condensation of a hydrazine with an aldehyde to yield a hydrazone. The next step is the coupling of a diazonium salt to the hydrazone, which affords the formazans in yields of 11−48% (Scheme 1, route A). A major disadvantage of this route is the limited stability of aryldiazonium salts, especially when sterically demanding 2,6-substituents are present. In search for a method to synthesize formazan ligands with more sterically demanding N−Ar substituents, we explored the coupling of hydrazines with hydrazonoyl chlorides (Scheme 1, route B). This method for the synthesis of formazan was already described by Pechmann in 1894[19] but has thereafter been used only sporadically.[20] The synthesis of ligands **L4H** and **L5H**, which we were unable to obtain using route A, was successfully accomplished with route B. Formazan **L4H** was prepared from the reaction of the corresponding *N*-phenylhydrazonoyl chloride with 2,6-diisopropylphenylhydrazine. Carrying out the reaction in EtOH under air resulted in *in situ* oxidation of the intermediate benzohydrazonohydrazide to form the desired formazan **L4H** in 34% yield after crystallization. Similarly, the symmetrical 2,6-dichlorophenyl-substituted formazan **L5H** was obtained via route B, albeit that the final step was relatively low-yielding (17%). In contrast to the formazan syntheses described above, the attempted preparation of a formazan with $R^1 = R^5$ = DIPP, a direct analogue of the symmetrical DIPP-substituted BDI ligand **A** (Chart 1), via route B was met with limited success.. Although it proved possible to obtain the desired product in low yield (see the Supporting Information for NMR spectral data), the purification was tedious and poorly reproducible in our hands.

Regardless, the synthesis of formazans via route B is a useful alternative to the commonly used diazonium coupling chemistry and may be extended to ligands for which diazonium precursors are not available (e.g., formazans with *N*-alkyl substituents). Finally, **L6H** was synthesized via the direct coupling of a diazonium compound to phenylpyruvic acid following a literature procedure.[21]

Complex Synthesis and Characterization. Mono(formazanate)zinc methyl complexes were obtained by treatment of the free ligands (**L1H**−**L6H**) with 1 equiv of dimethylzinc in toluene solution at room temperature (Scheme 2). Elongated reaction times are required for the more sterically hindered ligands (overnight), whereas **L1H** is fully converted in 30 min. Removal of the volatiles afforded the mono(formazanate)zinc complexes **1**−**6** in good yields. Crystals of **1**−**6** suitable for X-ray diffraction were obtained by cooling concentrated solutions of the mono(formazanate) zinc methyl complexes in toluene or hexane. For complexes that crystallized less readily (i.e., **4** and **5**), prolonged standing of the solutions resulted ultimately in the isolation of crystals of the corresponding bis(formazanate)zinc complexes (see the Supporting Information). To prevent ligand redistribution, crystallization was repeated in the presence of an additional 0.2 equiv of $ZnMe_2$ present in solution, and this allowed the isolation of **4** and **5** in pure, crystalline form. The X-ray data show that complexes **1**−**6** are present in the solid state as monomeric compounds with a three-coordinate Zn center surrounded by the bidentate formazanate ligand and a methyl group in an approximately trigonal-planar arrangement (Figures 1 and 2; pertinent metrical parameters in Table 1).

Compound **1** crystallizes with three independent, virtually planar molecules in the unit cell which show stacking in an alternating ("ABA") arrangement. The molecular planes

Scheme 2. Synthesis of Mono(formazanate)zinc Methyl Complexes

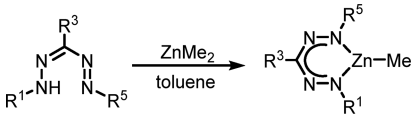

https://dx.doi.org/10.1021/acs.organomet.0c00720
Organometallics 2021, 40, 63−71

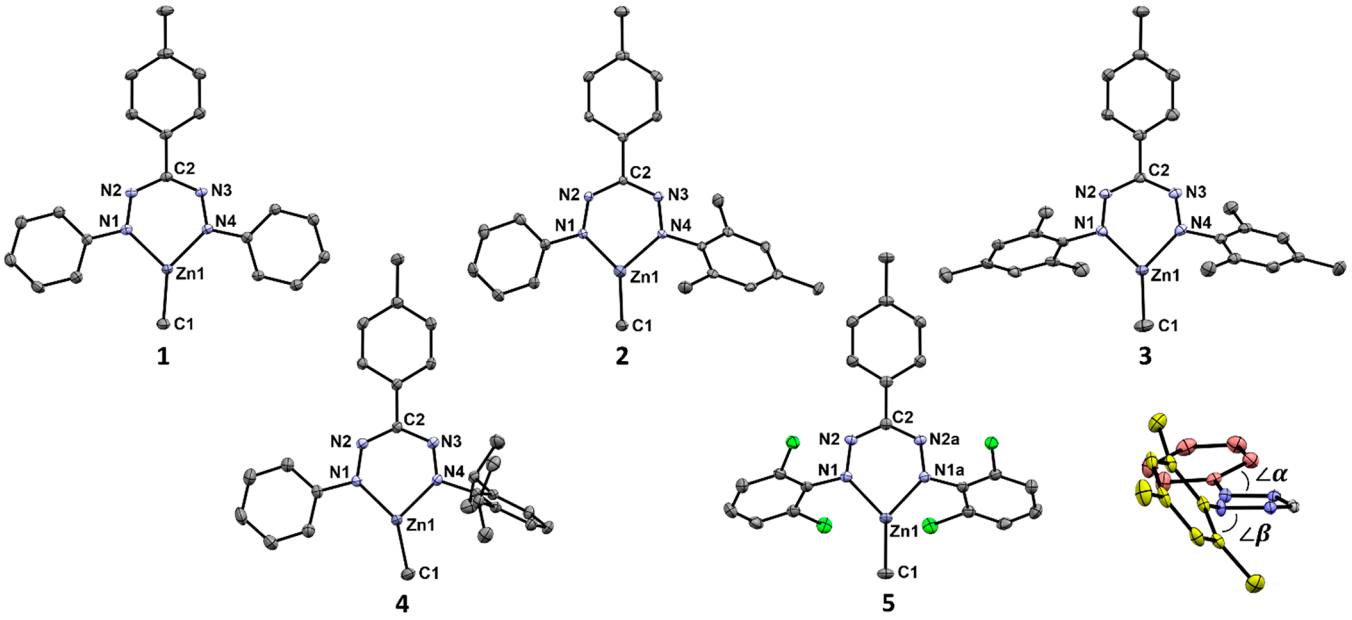

Figure 1. Molecular structures of **1**−**5** showing 50% probability ellipsoids. One of three (for **1**) or of two (for **2** and **3**) independent molecules is shown. Hydrogen atoms are omitted for clarity. The angles α and β are defined as the dihedral angle between the N−N vector and the least-squares plane of the attached aromatic ring.

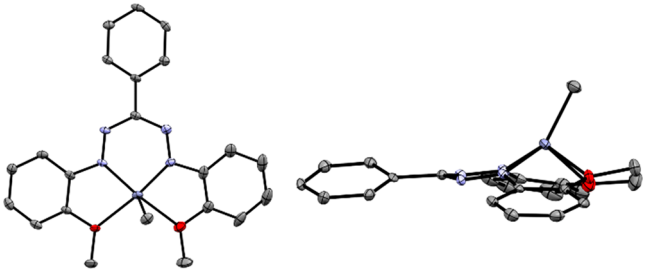

Figure 2. Molecular structure of **6** showing 50% probability ellipsoids. The toluene solvent molecule and hydrogen atoms are omitted for clarity.

(defined by the ZnN_4C ring) are coplanar with interplanar angles of 3.83° and 1.45° between adjacent molecules and distances between the Zn atoms and the neighboring molecular planes of <3.2 Å. In contrast, the presence of two sterically encumbering N-Mes substituents in compound **3** makes it distinctly nonplanar, and no intermolecular stacking is observed in the solid state. The solid-state structure of compound **5** shows a steplike stacking in neighboring molecules with a small interplanar separation of 3.27 Å for the ZnN_4C planes, with interactions between the methyl $ZnCH_3$ group and the chlorines of an adjacent molecule (Figure S31).

In all complexes, there is full charge delocalization over the NNCNN ligand backbone as indicated by the equivalent intraligand C−N and N−N bond lengths. Furthermore, with increasing size of the N−Ar groups these aryl rings rotate out of the ligand NNCNN plane to minimize steric interactions: whereas both N-Ph rings in **1** are essentially coplanar with the ligand backbone (dihedral angles α/β of 6.24° and 12.12°), the larger N-Mes group in **2** is rotated out of the plane (58.49°). A similar effect is seen in complex **3** with two N-Mes substituents, which are both oriented away from the ligand backbone with dihedral angles between the mesityl ring and the NNCNN plane of ∼62°. The out-of-plane rotation leads to loss of conjugation between the aromatic ring and the ligand backbone. Consequently, the nitrogen becomes a better donor, which is reflected in the shorter (average) Zn−N bond distances (1.996 vs 1.989 vs 1.972 Å, in **1**, **2**, and **3**, respectively). In contrast, the Zn−N bond length in compound **5** is somewhat longer (2.013 Å), suggesting it is a weaker

Table 1. Selected Bond Distances (Å) and Angles (deg) for Compounds 1−6

	1[a]	2[a]	3[a]	4	5[b]	6
Zn1−C1	1.956(3)	1.949(2)	1.945(5)	1.945(2)	1.943(3)	1.968(4)
Zn1−N1	2.003(2)	1.986(2)	1.968(3)	1.972(2)	2.013(2)	2.047(3)
Zn1−N4	1.989(2)	1.992(2)	1.976(3)	2.001(2)		2.033(3)
N1−N2	1.299(3)	1.303(2)	1.306(4)	1.311(3)	1.300(2)	1.302(4)
N3−N4	1.310(3)	1.300(2)	1.309(4)	1.297(3)		1.322(4)
N2−C2	1.346(2)	1.349(3)	1.348(4)	1.342(3)	1.351(2)	1.348(4)
N3−C2	1.337(3)	1.353(3)	1.345(4)	1.364(3)		1.350(4)
α	12.12	6.16	62.80	4.70	56.60	9.93
β	6.24	58.49	62.82	78.64		15.36

[a]Only one of the independent molecules is discussed. [b]The asymmetric unit of **5** contains half the molecule; the other half is generated by reflection in the mirror plane.

https://dx.doi.org/10.1021/acs.organomet.0c00720
Organometallics 2021, 40, 63−71

donor despite having a similar out-of-plane orientation of the N−Ar ring as in **3**, which is attributed to the electron-withdrawing Cl substituents. The Zn−C bond in these complexes is in the range 1.935−1.968 Å, which is comparable to the bond lengths in β-diketiminate zinc methyl complexes reported by Parkin et al.[22]

In compound **6** the OMe substituents on the N-Ar rings are weakly coordinated to Zn. The geometry around the zinc center is best described as pseudo-five-coordinate, with strong bonding interactions with both nitrogens of the formazanate ligand and the carbon of the methyl group, in a distorted trigonal arrangement, and additional weak interactions with the OMe groups (Zn−O1, 2.329 Å, and Zn−O2, 2.511 Å). Although the interaction between the Zn center and the OMe group in **6** appears to be relatively weak, the presence of the two additional donor sites can potentially stabilize **6** toward ligand redistribution reactions. At the same time, the solid-state structure of **6** shows that the Zn atom is significantly displaced out of the formazanate coordination plane (0.957 Å), making it still relatively accessible (Figure 2). An analogous copper complex of 1,5-bis(*o*-methoxyphenyl)-3-cyanoformazan was reported by Hicks, which also showed a pseudo-five-coordinate geometry with the Cu center raised 0.487 Å above the NNOO plane.[23]

In contrast to the coordination behavior observed with the tetradentate formazanate ligand **L6**, the related β-diketiminate ligand (2-OMe-C_6H_4NC(Me)CHC(Me)N(2-OMeC_6H_4), BDI-OMe) does not show coordination of the OMe groups to the metal center in the corresponding zinc amide or alkoxide complexes.[24] Similarly, a zinc ethyl complex with the BDI ligand 2-OMe-C_6H_4NC(Me)CHC(Me)N(2,6-^{i}PrC_6H_3) containing a single OMe donor also showed no propensity for Zn···OMe coordination.[25] Thus, it appears that formazanate anions are overall relatively poor donors, making the zinc center in these formazanate compounds more Lewis acidic than in the BDI analogues.

Cyclic Voltammetry. The redox chemistry of the mono(formazanate)zinc methyl complexes was evaluated by using cyclic voltammetry (Figure 3; redox potentials tabulated in Table 2). Compound **1** shows a quasi-reversible redox wave at

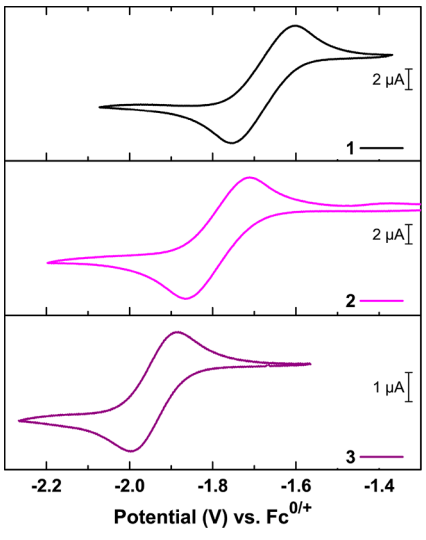

Figure 3. Cyclic voltammograms of **1**−**3** (1.5 mM solution in THF, 0.1 M [Bu_4N][PF_6]) recorded at 50 mV/s.

Table 2. Reduction Potentials and UV/Vis Absorption Maxima for Compounds 1−6

compound	$E_{1/2}$ (V vs Fc)	λ_{max} (nm)
1	−1.61	567
2	−1.81	503
3	−1.91	462
4	−1.78	487
5	−1.52	480
6	−1.69	606

−1.61 V and a second, less reversible reduction at −2.37 V (all potentials vs $Fc^{0/+}$; Figure S34). The first reduction at −1.61 V likely forms the radical anion $\mathbf{1}^{\bullet-}$, in which one electron is deposited in the formazanate ligand. Upon sweeping further to a more negative potential, a second reduction forms the two-electron-reduced complex $\mathbf{1}^{2-}$, which appears to have limited stability under these conditions, indicated by $I_{p,a}/I_{p,c} < 1$.

The cyclic voltammograms of compounds **1**−**3** show that the $LZnMe^{0/-}$ redox couple occurs at progressively more negative potentials (cathodic shifts of 200 and 300 mV for **2** and **3**, respectively). This can be attributed to the decreased conjugation between the formazanate NNCNN core and the N−Ar substituents (reflected in larger values for dihedral angles α/β in Table 1) that results from the steric pressure of the 2,6-substituents of the N-Ar groups.

In agreement with this notion is the observation that the reduction potential of **4** is very similar to that of **2**, despite the presence of more electron-donating isopropyl substituents. On the other hand, the 2,6-dichlorophenyl-substituted compound **5** shows a reduction potential of −1.52 V vs $Fc^{0/+}$, which is shifted *anodically* by 90 mV in comparison to **1**. It appears in this case that the Cl substituent is sufficiently electron-withdrawing that it more than compensates for the cathodic shift that is expected based on the out-of-plane orientation of the N−Ar rings in **5** ($\alpha = \beta = 56.60°$).

UV−Vis Spectroscopy. The optical properties of the mono(formazanate)zinc methyl complexes were measured by UV−vis absorption spectroscopy of the compounds in toluene solution. All compounds show intense absorption bands in the range 460−600 nm (Figure 4 and Table 2), similar to other formazanate complexes, which can be assigned to the $\pi-\pi^*$ transition of the conjugated system in the NNCNN backbone.[17a] When comparing λ_{max} of compounds **1** (567 nm), **2** (503 nm), and **3** (462 nm), a significant blue-shift in the absorption maximum is observed. We assign this blue-shift to the out-of-conjugation, perpendicular orientation of the aryl

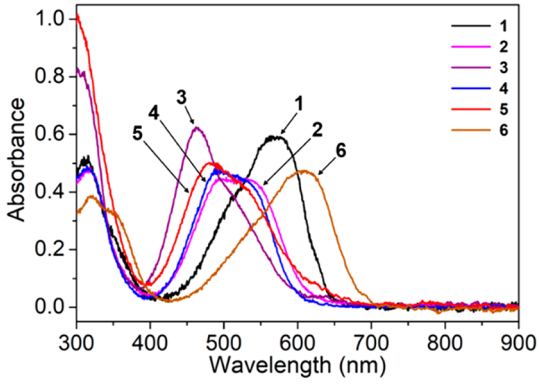

Figure 4. Absorption spectra of compounds **1**−**6** in toluene solution.

https://dx.doi.org/10.1021/acs.organomet.0c00720
Organometallics 2021, 40, 63−71

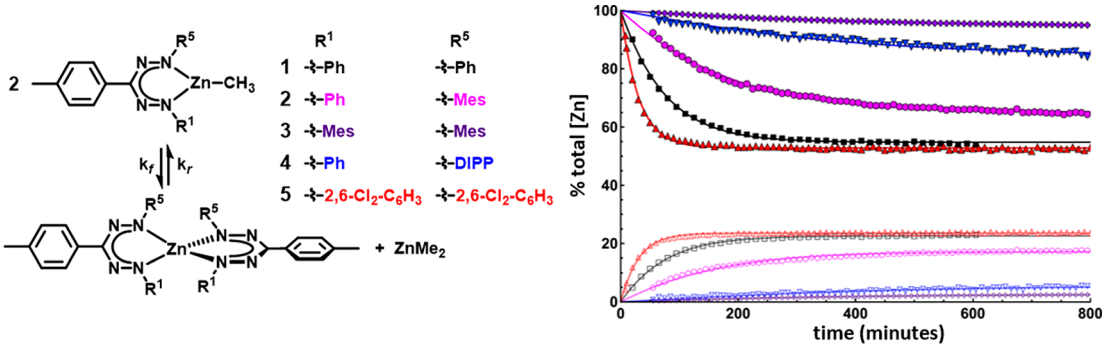

Figure 5. Kinetic traces of the approach to equilibrium of compounds **1**−**5** in C_6D_6 at 80 °C (black squares (**1**), magenta circles (**2**), purple diamonds (**3**), blue down triangle (**4**), and red up triangle (**5**)). Filled markers indicate the trace for the conversion of mono(formazanate)zinc methyl, and open markers signify the formation of bis(formazanate)zinc. Ph = phenyl, Mes = mesityl, DIPP = 2,6-diisopropylphenyl, and 2,6-Cl_2-C_6H_3 = 2,6-di(chloro)phenyl.

groups R^1 and R^5 with respect to the ligand core (indicated by large values for α/β in the solid-state structures; *vide supra*). This orientation is likely retained in solution and precludes π-conjugation between the NNCNN backbone and the N-Ar groups.

Compounds **4** and **5** show absorption bands that are very similar to those of **2**, as anticipated based on the structural data discussed above. Compound **6**, on the other hand, shows a significant red-shift and has an absorption maximum at 606 nm. This is in agreement with the planar geometry of the NNCNN backbone and its N-aryl substituents due to coordination of the *o*-OMe groups. Additionally, the oxygen lone pairs or the OMe group can be delocalized into the π-system to further increase planarity and lead to donor−acceptor character of the electronic transition as observed in the corresponding BF_2 complexes.[26]

Kinetics of Ligand Redistribution. To study the stability of compounds **1**−**5** toward ligand redistribution in solution, we monitored C_6D_6 solutions by ^{1}H NMR spectroscopy. An NMR sample of complex **1** left at room temperature was found to form a new formazanate-containing species and Me_2Zn over the course of several hours. Upon closer inspection, the new species was identified as the corresponding bis(formazanate) zinc complex.[15] Monitoring the NMR spectral changes at 80 °C in C_6D_6 solution showed that an equilibrium is established between **1** and the homoleptic analogues, with $K = 0.17$ based on ^{1}H NMR integration (Figure 5). Fitting the data to an approach to equilibrium for opposing bimolecular reactions[27] afforded the rate constants $k_f = 58.9\ M^{-1}\ min^{-1}$ and $k_r = 345.4\ M^{-1}\ min^{-1}$. The ligand redistribution reactions for the other compounds were measured in the same manner, allowing a comparison of the reaction rates and equilibrium constants within the series (Table 3). As expected, the largest extent of conversion to the homoleptic complexes is observed for the (formazanate)zinc methyl complex **1**, which has the least sterically demanding substituents (N-Ph). Increasing the size of the N-Ar substituents results in an equilibrium composition that is shifted more to the mono(formazanate) zinc complexes, such that for the most hindered complex **3** (with two N-Mes groups) the equilibrium constant is $<10^{-3}$. Even after several days at 80 °C, no further conversion of **3** is observed, indicating that sterically demanding ligands effectively shut down ligand redistribution in these three-coordinate complexes by destabilizing the bis(formazanate) zinc products. This is reflected in the Gibbs free energy change (ΔG) at 80 °C, which increases from 5.2 to 21.1 kJ/mol on going from **1** to **3**. Based on these measurements, the asymmetric ligand in **4** (N-Ph/N-DIPP substituents) is more prone to ligand redistribution than the symmetric complex **3** (N-Mes), with a difference in equilibrium thermodynamics ($\Delta\Delta G$) of ca. 5.9 kJ/mol. Monitoring the ligand redistribution for the 2,6-dichlorophenyl-substituted complex **5** shows that it has the highest reaction rate within the series and reaches an equilibrium that favors the homoleptic species the most (K = 0.20). Thus, in addition to steric effects there is a substantial contribution from electronic perturbations due to the electron-withdrawing *ortho*-chloro substituents in **5**. With regard to the electron-donating *ortho*-methoxy groups in complex **6**, it was hypothesized that OMe groups would stabilize the mono-(formazanate)zinc methyl species by coordination to the Zn center. Indeed, when an NMR sample of **6** was heated to 80 °C, the formation of the corresponding bis(formazanate)zinc complex was not observed. Moreover, compound **6** was found to be stable even in the presence of excess ligand **L6H**, indicating that the additional MeO···Zn interaction makes **6** substantially more stable than the three-coordinate zinc methyl complexes. It should be noted that, in contrast to **6**, the corresponding diketiminate complex [BDI-OMe]ZnEt was reported to slowly disproportionate into $[BDI\text{-}OMe]_2Zn$ and $ZnEt_2$.[24b] This difference may be attributed to the lower propensity of MeO···Zn interactions in the (BDI)ZnR complexes; the Zn center in BDI complexes is apparently less Lewis acidic due to the stronger donor ability of diketiminate ligands in comparison to formazanates.

When the ligand redistribution of complex **1** was monitored by ^{1}H NMR in the more polar solvent THF-d_8, the formation of the homoleptic species was suppressed significantly. Although k_f is not affected much by the change in solvent, k_r for complex **1** is ca. 20 time larger in THF-d_8 than in C_6D_6,

Table 3. Equilibrium and Rate Constants for the Approach to Equilibrium

compound	K_{eq}	ΔG^0 (kJ/mol)	k_f (M^{-1} min^{-1})	k_r (M^{-1} min^{-1})
1	0.17	5.2	58.9	345
1 (THF)	4.0×10^{-3}	16.2	24.2	6075
2	0.071	7.8	19.6	277
3	7.6×10^{-4}	21.1	1.21	1590
4	5.9×10^{-3}	15.1	3.04	514
5	0.20	4.7	150	755

https://dx.doi.org/10.1021/acs.organomet.0c00720
Organometallics 2021, 40, 63−71

resulting in a much smaller equilibrium constant (K_{eq} = 4.0 × 10^{-3}). This may be attributed to the formation of a more stable four-coordinate THF adduct in solution.

Steric Maps and Buried Volume. By calculation of the buried volume (V_{bur}) based on the solid-state structures of complexes **1**−**6**, the steric pressure exerted by the ligands was quantified.[28] The effect of the N-Ar substituents on the steric environment can be visualized by steric maps shown in Figure 6, where the introduction of one or two mesityl groups (**2** and **3**, respectively) results in an increased occupancy of the first coordination sphere around the zinc center with %V_{bur} increasing from 43.9 (**1**) to 47.9 (**2**) to 51.5 (**3**). This increase in V_{bur} is correlated to the increased stability of the mono(formazanate)zinc methyl complexes, represented by a higher ΔG for the equilibrium reaction (Figure 7). Compound **4** also follows this trend, as the V_{bur} of 49.7% is in between that of **2** and **3**, congruent with a ΔG of 15.1 kJ/mol.

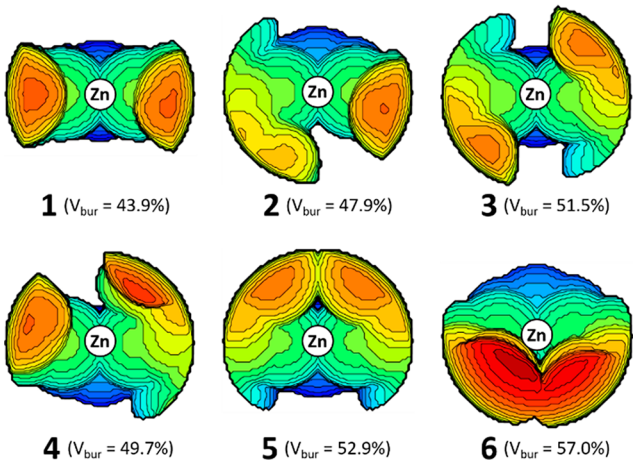

Figure 6. Steric maps and buried volumes of the ligands in complexes **1**−**6**. Showing a 3.5 Å sphere around the Zn atom, blue is to the rear and red to the front of the metal.

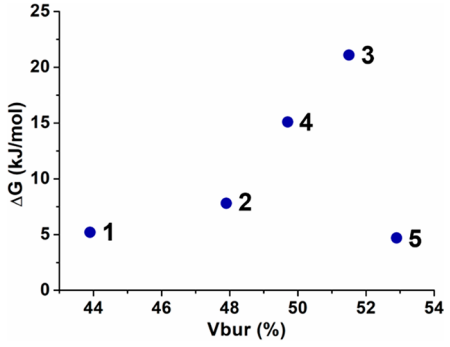

Figure 7. Correlation between V_{bur} and the Gibbs free energy change (ΔG) at 80 °C.

A similar analysis for **5** shows that it has the highest V_{bur} in the series (52.9%). However, as observed in the characterization data discussed above, the electronic effect of the chlorine distinguishes it from the others, and this is also reflected in **5** breaking the trend between V_{bur} and ΔG (Figure 7). For compound **6**, the steric map clearly shows that the coordination of the OMe and the displacement of Zn out of the NNOO plane (*vide supra*) effectively shield access to the zinc center from one side, which results in a high V_{bur} of 57.0%.

CONCLUSIONS

The influence of the steric environment around the zinc center, introduced by the formazanate ligand, on the stability of mono(formazanate)zinc methyl complexes was investigated. The equilibrium between the mono(formazanate)zinc methyl complexes and the corresponding homoleptic species can be related to the steric effects of the aromatic groups. More sterically demanding N-Ar substituents shift the equilibrium to favor the mono(formazanate)zinc methyl species and retard the forward reaction. However, it appears that electronic factors are also of importance for the rate of approach to equilibrium, with electron-withdrawing groups exhibiting an increased reaction rate. Examination of the solid-state structures of complexes **1**−**6** revealed that the presence of substituents on the *ortho*-position of the aromatic ring induces an out-of-plane twist of the aromatic group. This rotation of the N-Ar groups out of the NNCNN plane leads to a loss of conjugation of the Ar substituents with the NNCNN backbone. The effect of this loss of conjugation can be observed in the electronic and optical properties, where a blue-shift was observed in the absorption spectra. A similar trend is observed for the redox properties, with more cathodic potentials required for the first reduction upon going from **1** to **3**. However, electronic properties can override this effect as the first reduction of complex **5** is shifted anodically by 90 mV in comparison to **1**, which is attributed to the electron withdrawing effect of the chloride substituents. The Gibbs free energy change of the ligand redistribution reaction was found to be correlated to the "buried volume" (a measure of the ligand steric properties), showing that the ligand environment around the zinc center has a significant influence on the kinetics and thermodynamics of the ligand redistribution. In addition to stabilizing three-coordinate (formazanate)zinc methyl complexes via steric effects, the introduction of additional OMe donor groups as substituents in complex **6** is shown to completely suppress ligand exchange.

EXPERIMENTAL SECTION

General Considerations. All manipulations, except for ligand synthesis, were performed under a nitrogen atmosphere by using glovebox, Schlenk, and vacuum-line techniques. Glassware was dried before use at 150 °C. The reagents used for the synthesis of ligands **L1H**, **L2H**, **L3H**, **L4H**, **L5H**, and **L6H** were used as received; 2,6-diisopropyl-1-bromobenzene (Fluorochem & ABCR), Mg turnings (Acros), di-*tert*-butyl azodicarboxylate (Fluorochem & Sigma-Aldrich), CCl_4 (Acros), PPh_3 (Merck), Et_3N (Sigma-Aldrich), dimethyl sulfide (Sigma-Aldrich), *N*-chlorosuccinimide (Sigma-Aldrich), *p*-tolualdehyde (Sigma-Aldrich), *p*-toluoyl chloride (Sigma-Aldrich), phenylhydrazine (Sigma-Aldrich), and 2,6-dichlorophenylhydrazine hydrochloride (Fluorochem). The ligands **L1H**,[18] **L2H**,[18], **L3H**,[18] and **L6H**[21] were synthesized via literature procedures. Toluene and hexane (Sigma-Aldrich, anhydrous, 99.8%) were passed over columns of Al_2O_3 (Fluka), BASF R3-11-supported Cu oxygen scavenger, and molecular sieves (Sigma-Aldrich, 4 Å). THF (Sigma-Aldrich, anhydrous, 99.8%) was dried by percolation over columns of Al_2O_3 (Fluka). Deuterated solvents were vacuum transferred from the Na/K alloy (C_6D_6, toluene-d_8, THF-d_8, Euriso-top) and stored under nitrogen. Dimethylzinc (Sigma-Aldrich, 2.0 M in toluene or ABCR, 10 wt % in hexane) was used as received.

NMR spectra were recorded on Agilent 400 MR, Varian Mercury Plus 400, Varian Inova 500, or Bruker Avance NEO 600 spectrometers. The ^1H and ^{13}C NMR spectra were referenced

https://dx.doi.org/10.1021/acs.organomet.0c00720
Organometallics 2021, 40, 63−71

internally by using the residual solvent resonances and reported in ppm relative to TMS (0 ppm). Electrochemical measurements were performed under an inert N_2 atmosphere in a glovebox by using an Autolab PGSTAT 204 computer-controlled potentiostat. Data were recorded with an Autolab NOVA software (ver. 2.1.4). Cyclic voltammetry (CV) was performed by using a three-electrode configuration comprised of a Pt wire counter electrode, a Ag wire pseudoreference electrode, and a Pt disk working electrode (CHI102, CH Instruments, diameter = 2 mm). The Pt working electrode was polished before experiment using alumina slurry (0.05 μm), rinsed with distilled water, and subjected to brief ultrasonication to remove any adhered alumina microparticles. The electrodes were then dried in an oven at 75 °C overnight to remove any residual traces of water. The CV data were calibrated by adding ferrocene to the THF solution at the end of experiments. In all cases, there is no indication that addition of ferrocene influences the electrochemical behavior of products. All electrochemical measurements were performed at ambient temperatures under an inert N_2 atmosphere in THF containing 0.1 M $[Bu_4N][PF_6]$ as the supporting electrolyte. UV/vis spectra were recorded in a toluene solution ($\approx 10^{-5}$ M) by using an Avantes AvaSpec-2048 UV/vis spectrophotometer.

Synthesis of 1-(Phenyl)-5-(2,6-diisopropylphenyl)-3-(*p*-tolyl)formazan [L4H]. *N*′-(Phenyl)-4-methylbenzohydrazonoyl chloride (1.018 g, 4.16 mmol) was dissolved in 50 mL of EtOH (100%), and triethylamine (0.993 g, 9.81 mmol) was added to the mixture. The solution was stirred, and (2,6-diisopropylphenyl)-hydrazine HCl was added in portions (1.001 g in total, 4.38 mmol). The reaction was stirred overnight, and the volatiles were removed under reduced pressure. The resulting dark red oil was dissolved in ethyl acetate, and the suspension that formed was filtered. The filtrate was concentrated under reduced pressure to a sticky oil, to which 3 mL of DCM was added, which was layered with methanol and put in a freezer at −30 °C. After 3 days the layers had mixed and crystals had formed, which were filtered off, washed with cold methanol, and dried in vacuo. The product was obtained as dark red crystals (571 mg, 1.43 mmol, 34.4%). ^{1}H NMR (400 MHz, $CDCl_3$, 25 °C): δ 14.94 (s, 1H), 7.99 (d, 2H), 7.60 (d, 2H), 7.43 (t, 2H), 7.31 (s, 3H), 7.25−7.19 (m, 3H), 3.30 (sept, 2H), 2.41 (s, 3H) 1.28 (d, 12H) ppm. ^{13}C NMR (151 MHz, $CDCl_3$, 25 °C): δ 146.75, 144.62, 138.17, 137.36, 131.29, 130.74, 129.57, 129.30, 125.84, 125.54, 117.28, 21.41, 21.22, 21.11 ppm. MS (ESI, negative mode): exact mass calculated for $[C_{26}H_{29}N_4]^-$: 397.2398; exact mass found: 397.2403; difference: + 1.3 ppm.

Synthesis of 1,5-Bis(2,6-dichlorophenyl)-3-(*p*-tolyl)-formazan [L5H]. (2,6-Diisopropylphenyl)hydrazine HCl (200 mg, 0.94 mmol) was added to 10 mL of EtOH (100%) to give a suspension; addition of triethylamine (127 mg, 1.26 mmol) dissolved all solids and afforded a clear solution. The solution was stirred, and *N*′-(2,6-dichlorophenyl)-4-methylbenzohydrazonoyl chloride (220 mg, 0.70 mmol) was added, after which a very gradual color change was noticeable. The reaction was stirred overnight, and the next day the reaction mixture had turned deep red. The volatiles were removed under reduced pressure, resulting in a dark red oil which was dissolved in minimal DCM, layered with methanol, and placed in a freezer at −30 °C. After 4 days the layers had diffused into each other, and crystals had formed. Dark red crystals were collected, washed with methanol, and dried in vacuo to give 38 mg of **L5H**. The filtrate was concentrated under reduced pressure to a sticky oil, to which 3 mL of DCM was added, which was layered with methanol and put in a freezer at −30 °C. After 3 days the layers had mixed, and crystals had formed, which were isolated, washed with cold methanol, and dried in vacuo to give another 32 mg of product. The total yield of **L5H** was 70 mg (0.155 mmol, 17%). ^{1}H NMR (400 MHz, $CDCl_3$, 25 °C): δ 13.99 (s, 1H), 7.99 (d, 2H), 7.42 (d, 4H), 7.24 (d, 2H), 7.13 (t, 2H), 2.40 (s, 3H) ppm. ^{13}C NMR (101 MHz, $CDCl_3$, 25 °C): δ 143.65, 141.99, 138.25, 133.43, 129.73, 129.35, 127.58, 127.43, 126.37, 21.47 ppm. MS (ESI, negative mode): exact mass calculated for $[C_{20}H_{13}N_4Cl_4]^-$: 450.9870; exact mass found: 450.9872; difference: + 0.4 ppm.

General Procedure for the Synthesis of Mono-(formazanate)zinc Methyl Complexes. Formazan was dissolved in toluene, and 1.2 equiv of dimethylzinc (as a 2.0 M solution in toluene) was added at room temperature with stirring. After the appropriate reaction time (given for each compound below), the volatiles were removed under reduced pressure. The solid product was isolated and analyzed by NMR spectroscopy, which indicated full conversion to the desired product. The bulk purity of the solids was established by elemental analysis. Crystals suitable for X-ray diffraction were subsequently obtained as indicated below.

[PhNNC(*p*-tolyl)NNPh]ZnMe [1]. PhNNC(*p*-tolyl)NNHPh (715 mg, 2.27 mmol) was reacted in 20 mL of toluene with Me_2Zn for 30 min. A color change was observed from dark red to dark violet concurrent with gas evolution. Removal of the volatiles under reduced pressure gave 705 mg of a dark blue powder (1.79 mmol, 89% yield). Crystals suitable for X-ray diffraction were obtained by cooling a concentrated toluene solution to −30 °C. ^{1}H NMR (400 MHz, C_6D_6, 25 °C): δ 8.34 (d, 2H, *p*-tol *o*-CH), 7.83 (d, 4H, Ph *o*-CH), 7.31 (d, 2H, *p*-tol *m*-CH), 7.20 (t, 4H, Ph *m*-CH), 7.04 (t, 2H, Ph *p*-CH), 2.27 (s, 3H, *p*-tol *p*-CH_3), −0.13 (s, 3H, Zn-CH_3) ppm. ^{13}C NMR (126 MHz, C_6D_6, 25 °C): δ 154.01, 144.11, 137.93, 136.92, 129.68, 129.44, 127.71, 126.20, 121.12, 21.29, −9.02 ppm. Anal. Calcd for $C_{21}H_{20}N_4Zn$: C 64.05, H 5.12, N 14.23; found: C 64.44, H 5.16, N 13.93.

[PhNNC(*p*-tolyl)NNMes]ZnMe [2]. PhNNC(*p*-tolyl)NNHMes (70 mg, 0.20 mmol) was reacted in 3 mL of toluene with Me_2Zn for 3 h. A color change was observed from deep red to violet concurrent with gas evolution. Removal of the volatiles under reduced pressure afforded 57 mg of **2** (0.13 mmol, 66% yield). Crystals were obtained by cooling a concentrated toluene solution to −30 °C. ^{1}H NMR (400 MHz, C_6D_6, 25 °C): δ 8.30 (d, 2H, *p*-tol *o*-CH), 7.95 (d, 2H, Ph *o*-CH), 7.24−7.18 (m, 4H, *p*-tol *m*-CH and Ph *m*-CH), 7.03 (t, 1H, Ph *p*-CH), 6.74 (s, 2H, Mes *m*-CH), 2.21 (s, 3H, *p*-tol *p*-CH_3), 2.10 (s, 3H, Mes *p*-CH_3), 2.05 (6H, Mes *o*-CH_3), −0.28 (br s, 3H, Zn−CH_3) ppm. ^{13}C NMR (101 MHz, C_6D_6, 25 °C): δ 154.20, 149.06, 145.15, 137.27, 137.04, 136.70, 130.62, 130.10, 129.71, 129.69, 127.51, 125.81, 120.80, 21.23, 20.92, 18.64, −12.98 ppm. Anal. Calcd for $C_{24}H_{26}N_4Zn$: C 66.13, H 6.01, N 12.85; found: C 65.99, H 6.01, N 12.71.

[MesNNC(*p*-tolyl)NNMes]ZnMe [3]. MesNNC(*p*-tolyl)-NNHMes (50 mg, 0.125 mmol) was reacted in 3 mL of toluene with Me_2Zn for 18 h, during which the solution took on a light orange color. Removal of the volatiles afforded 40 mg of **3** (0.084 mmol, 67% yield). Crystals suitable for X-ray analysis were obtained by slow evaporation of C_6D_6. ^{1}H NMR (600 MHz, C_6D_6, 25 °C): δ 8.23 (d, 2H, *p*-tol *o*-CH), 7.13 (d, 2H, *p*-tol *m*-CH), 6.78 (s, 4H, Mes CH), 2.17 (s, 12H, Mes *o*-CH_3), 2.14 (s, 3H, *p*-tol CH_3), 2.12 (6H, Mes *p*-CH_3), −0.38 (br. s, 3H, Zn−CH_3) ppm. ^{13}C NMR (151 MHz, C_6D_6, 25 °C): δ 149.08, 145.78, 136.97, 136.93, 136.56, 130.71, 130.22, 129.70, 125.35, 21.15, 20.93, 18.75, −15.61 ppm. Anal. Calcd for $C_{27}H_{32}N_4Zn$: C 67.85, H 6.75, N 11.72; found: C 67.87, H 6.87, N 11.61.

[DiPPNNC(*p*-tolyl)NNPh]ZnMe [4]. PhNNC(*p*-tolyl)NNHDiPP (126 mg, 0.32 mmol) was reacted in 6 mL of toluene with Me_2Zn for 6 h, leading to a magenta solution, which upon removal of the volatiles afforded 116 mg of **4** (0.24 mmol, 76% yield). Crystallization was achieved by slow diffusion of hexane into a concentrated toluene solution containing the product and a drop of dimethylzinc to prevent the formation of the bis(formazanate)zinc complex. ^{1}H NMR (400 MHz, C_6D_6, 25 °C): δ 8.29 (d, 2H, *p*-tol *o*-CH), 7.98 (d, 2H, Ph *o*-CH), 7.22−7.17 (m, 5H*, *p*-tol *m*-CH and Ph *m*-CH and DIPP *p*-CH), 7.12 (d, 2H, DIPP *m*-CH), 7.01 (t, 1H, Ph *p*-CH), 2.88 (sept, 2H, DIPP C$\underline{H}$(CH_3)$_2$), 2.19 (s, 3H, *p*-tol *p*-CH_3), 1.09 (d, 12H, DIPP CH(C$\underline{H}_3$)$_2$), −0.27 (br s, 3H, Zn−CH_3) ppm *(overlapping with solvent). ^{13}C NMR (101 MHz, C_6D_6, 25 °C): δ 154.12, 148.42, 145.27, 141.82, 137.12, 137.02, 129.78, 129.73, 127.58, 125.79, 123.99, 120.71, 28.71, 24.66, 23.18, 21.21, −14.19 ppm. Anal. Calcd for $C_{27}H_{32}N_4Zn$: C 67.85, H 6.75, N 11.72; found: C 67.90, H 6.79, N 11.70.

https://dx.doi.org/10.1021/acs.organomet.0c00720
Organometallics 2021, 40, 63−71

[2,6-DiCl-PhNNC(*p*-tolyl)NN-2,6-DiCl-Ph]ZnMe [5]. 2,6-DiCl-PhNNC(*p*-tolyl)NN-2,6-diCl-Ph (24 mg, 0.053 mmol) was reacted in 1 mL of toluene with Me_2Zn for 6 h, which gave a deep red solution. Subsequent removal of the volatiles afforded 18 mg of **5** (0.034 mmol, 64% yield). Crystals suitable for X-ray analysis were grown by cooling a concentrated hexane solution, to which a drop of $ZnMe_2$ solution was added to prevent the formation of the bis(formazanate)zinc complex, to −30 °C. ^{1}H NMR (600 MHz, C_6D_6, 25 °C): δ 8.31 (d, 2H, *p*-tol *o*-CH), 7.14 (d, 2H, *p*-tol *m*-CH), 6.90 (d, 4H, $PhCl_2$ + *m*-CH), 6.34 (t, 2H, $PhCl_2$ + *p*-CH), 2.12 (s, 3H, *p*-tol *p*-CH_3), −0.29 (s, 3H, Zn−CH_3) ppm. ^{13}C NMR (151 MHz, C_6D_6, 25 °C): δ 147.05, 146.64, 137.60, 136.06, 129.76, 129.69, 129.39, 128.35, 125.90, 21.19, −14.98 ppm. Anal. Calcd for $C_{21}H_{16}Cl_4N_4Zn$: C 47.45, H 3.03, N 10.54; found: C 47.15, H 3.01, N 10.41.

[2-MeO-PhNNC(Ph)NN-2-MeO-Ph]ZnMe [6]. 2-MeO-PhNNC(Ph)NN-2-MeO-Ph (77.4 mg, 0.215 mmol) was reacted in 2.5 mL of toluene (2.5 mL) with Me_2Zn for 6 h, which gave a deep blue solution. Removal of the volatiles afforded 69.3 mg of **6** (0.153 mmol, 71% yield). Crystals were grown by slow diffusion of hexane into a toluene layer containing the product at −30 °C. ^{1}H NMR (400 MHz, C_6D_6, 25 °C): δ 8.38 (d, 2H, Ph *o*-CH), 8.35 (dd, 2H, 2-MeO−Ph H^6), 7.39 (t, 2H, Ph *m*-CH), 7.25 (t, 1H, Ph *p*-CH), 6.92 (quin of doub, 4H, 2-MeO-Ph H^4 and H^5), 6.44 (dd, 2H, 2-MeO−Ph H^3), 3.29 (s, 6H, OCH_3), −0.42 (s, 3H, Zn-CH_3) ppm. ^{13}C NMR (101 MHz, C_6D_6, 25 °C): δ 150.36, 146.42, 142.32, 139.39, 128.61, 127.53, 127.33, 126.03, 123.04, 118.19, 111.63, 55.68, −15.77 ppm. Anal. Calcd for $C_{22}H_{22}N_4O_2Zn$: C 60.08, H 5.04, N 12.74; found: C 60.16, H 5.26, N 12.14.

■ ASSOCIATED CONTENT

Supporting Information

The Supporting Information is available free of charge at https://pubs.acs.org/doi/10.1021/acs.organomet.0c00720.

Crystallographic data for **1**−**6**, $[L4]_2Zn$, and $[L5]_2Zn$ (CIF) NMR spectra and additional experimental data (PDF)

Accession Codes

CCDC 2033361−2033368 contain the supplementary crystallographic data for this paper. These data can be obtained free of charge via www.ccdc.cam.ac.uk/data_request/cif, or by emailing data_request@ccdc.cam.ac.uk, or by contacting The Cambridge Crystallographic Data Centre, 12 Union Road, Cambridge CB2 1EZ, UK; fax: +44 1223 336033.

■ AUTHOR INFORMATION

Corresponding Author

Edwin Otten − *Stratingh Institute for Chemistry, University of Groningen, 9747 AG Groningen, The Netherlands;* orcid.org/0000-0002-5905-5108; Email: edwin.otten@rug.nl

Authors

Folkert de Vries − *Stratingh Institute for Chemistry, University of Groningen, 9747 AG Groningen, The Netherlands*

Raquel Travieso-Puente − *Stratingh Institute for Chemistry, University of Groningen, 9747 AG Groningen, The Netherlands*

Peter Roewen − *Stratingh Institute for Chemistry, University of Groningen, 9747 AG Groningen, The Netherlands*

Complete contact information is available at: https://pubs.acs.org/10.1021/acs.organomet.0c00720

Notes

The authors declare no competing financial interest.

■ ACKNOWLEDGMENTS

Financial support from The Netherlands Organisation of Scientific Research (NWO) is gratefully acknowledged.

■ REFERENCES

(1) Gladysz, J. A.; Bedford, R. B.; Fujita, M.; Gabbaï, F. P.; Goldberg, K. I.; Holland, P. L.; Kiplinger, J. L.; Krische, M. J.; Louie, J.; Lu, C. C.; Norton, J. R.; Petrukhina, M. A.; Ren, T.; Stahl, S. S.; Tilley, T. D.; Webster, C. E.; White, M. C.; Whiteker, G. T. Organometallics Roundtable 2013−2014. *Organometallics* **2014**, *33*, 1505−1527.

(2) (a) Parks, J. E.; Holm, R. H. The Synthesis, Solution Stereochemistry, and Electron Delocalization Properties of Bis(β-iminoamino)nickel(II) Complexes. *Inorg. Chem.* **1968**, *7*, 1408−1416. (b) Bonnett, R.; Bradley, D. C.; Fisher, K. J.; Rendall, I. F. Metallo-Organic Compounds Containing Metal-Nitrogen Bonds. Part VII. Synthesis and Properties of Bis-(NN′-diethylbutane-1,3-di-iminato) Derivatives of Cobalt(II)2 and Zinc. *J. Chem. Soc. A* **1971**, *0*, 1622−1627.

(3) Bourget-Merle, L.; Lappert, M. F.; Severn, J. R. The Chemistry of β-Diketiminatometal Complexes. *Chem. Rev.* **2002**, *102*, 3031−3066.

(4) Intemann, J.; Sirsch, P.; Harder, S. Comparison of Hydrogen Elimination from Molecular Zinc and Magnesium Hydride Clusters. *Chem. - Eur. J.* **2014**, *20*, 11204−11213.

(5) (a) Green, S. P.; Jones, C.; Stasch, A. Stable Magnesium(I) Compounds with Mg-Mg Bonds. *Science* **2007**, *318*, 1754−1757. (b) Jones, C. Dimeric Magnesium(I) β-Diketiminates: A New Class of Quasi-Universal Reducing Agent. *Nat. Rev. Chem.* **2017**, *1*, 0059.

(6) Webster, R. L. β-Diketiminate Complexes of the First Row Transition Metals: Applications in Catalysis. *Dalton Trans.* **2017**, *46*, 4483−4498.

(7) (a) Biyikal, M.; Löhnwitz, K.; Meyer, N.; Dochnahl, M.; Roesky, P. W.; Blechert, S. β-Diketiminate Zinc Complexes for the Hydroamination of Alkynes. *Eur. J. Inorg. Chem.* **2010**, *2010*, 1070−1081. (b) Bernoud, E.; Oulié, P.; Guillot, R.; Mellah, M.; Hannedouche, J. Well-Defined Four-Coordinate Iron(II) Complexes For Intramolecular Hydroamination of Primary Aliphatic Alkenylamines. *Angew. Chem., Int. Ed.* **2014**, *53*, 4930−4934.

(8) Espinal-Viguri, M.; King, A. K.; Lowe, J. P.; Mahon, M. F.; Webster, R. L. Hydrophosphination of Unactivated Alkenes and Alkynes Using Iron(II): Catalysis and Mechanistic Insight. *ACS Catal.* **2016**, *6*, 7892−7897.

(9) Chen, C.; Hecht, M. B.; Kavara, A.; Brennessel, W. W.; Mercado, B. Q.; Weix, D. J.; Holland, P. L. Rapid, Regioconvergent, Solvent-Free Alkene Hydrosilylation with a Cobalt Catalyst. *J. Am. Chem. Soc.* **2015**, *137*, 13244−13247.

(10) (a) Cheng, M.; Attygalle, A. B.; Lobkovsky, E. B.; Coates, G. W. Single-Site Catalysts for Ring-Opening Polymerization: Synthesis of Heterotactic Poly(lactic acid) from rac-Lactide. *J. Am. Chem. Soc.* **1999**, *121*, 11583−11584. (b) Chamberlain, B. M.; Cheng, M.; Moore, D. R.; Ovitt, T. M.; Lobkovsky, E. B.; Coates, G. W. Polymerization of Lactide with Zinc and Magnesium β-Diiminate Complexes: Stereocontrol and Mechanism. *J. Am. Chem. Soc.* **2001**, *123*, 3229−3238.

(11) (a) Cheng, M.; Lobkovsky, E. B.; Coates, G. W. Catalytic Reactions Involving C1 Feedstocks: New High-Activity Zn(II)-Based Catalysts for the Alternating Copolymerization of Carbon Dioxide and Epoxides. *J. Am. Chem. Soc.* **1998**, *120*, 11018−11019. (b) Cheng, M.; Moore, D. R.; Reczek, J. J.; Chamberlain, B. M.; Lobkovsky, E. B.; Coates, G. W. Single-Site β-Diiminate Zinc Catalysts for the Alternating Copolymerization of CO_2 and Epoxides: Catalyst Synthesis and Unprecedented Polymerization Activity. *J. Am. Chem. Soc.* **2001**, *123*, 8738−8749. (c) Moore, D. R.; Cheng, M.; Lobkovsky, E. B.; Coates, G. W. Mechanism of the Alternating Copolymerization of Epoxides and CO_2 Using β-Diiminate Zinc Catalysts: Evidence for a Bimetallic Epoxide Enchainment. *J. Am. Chem. Soc.* **2003**, *125*, 11911−11924.

(12) (a) Baek, Y.; Betley, T. A. Catalytic C-H Amination Mediated by Dipyrrin Cobalt Imidos. *J. Am. Chem. Soc.* **2019**, *141*, 7797−7806. (b) Carsch, K. M.; DiMucci, I. M.; Iovan, D. A.; Li, A.; Zheng, S.-L.; Titus, C. J.; Lee, S. J.; Irwin, K. D.; Nordlund, D.; Lancaster, K. M.; Betley, T. A. Synthesis of a Copper-Supported Triplet Nitrene Complex Pertinent to Copper-Catalyzed Amination. *Science* **2019**, *365*, 1138−1143. (c) Dong, Y.; Lukens, J. T.; Clarke, R. M.; Zheng, S.-L.; Lancaster, K. M.; Betley, T. A. Synthesis, Characterization and C-H Amination Reactivity of Nickel Iminyl Complexes. *Chemical Science* **2020**, *11*, 1260−1268. (d) Wilding, M. J. T.; Iovan, D. A.; Betley, T. A. High-Spin Iron Imido Complexes Competent for C-H Bond Amination. *J. Am. Chem. Soc.* **2017**, *139*, 12043−12049.

(13) Ballmann, G.; Grams, S.; Elsen, H.; Harder, S. Dipyrromethene and β-Diketiminate Zinc Hydride Complexes: Resemblances and Differences. *Organometallics* **2019**, *38*, 2824−2833.

(14) Gilroy, J. B.; Ferguson, M. J.; McDonald, R.; Patrick, B. O.; Hicks, R. G. Formazans as β-Diketiminate Analogues. Structural Characterization of Boratatetrazines and Their Reduction to Borataverdazyl Radical Anions. *Chem. Commun.* **2007**, 126−128.

(15) Chang, M. C.; Dann, T.; Day, D. P.; Lutz, M.; Wildgoose, G. G.; Otten, E. The Formazanate Ligand as an Electron Reservoir: Bis(Formazanate) Zinc Complexes Isolated in Three Redox States. *Angew. Chem., Int. Ed.* **2014**, *53*, 4118−4122.

(16) Gilroy, J. B.; Otten, E. Formazanate Coordination Compounds: Synthesis, Reactivity, and Applications. *Chem. Soc. Rev.* **2020**, *49*, 85−113.

(17) (a) Chang, M. C.; Roewen, P.; Travieso-Puente, R.; Lutz, M.; Otten, E. Formazanate Ligands as Structurally Versatile, Redox-Active Analogues of β-diketiminates in Zinc Chemistry. *Inorg. Chem.* **2015**, *54*, 379−388. (b) Milocco, F.; de Vries, F.; Dall'Anese, A.; Rosar, V.; Zangrando, E.; Otten, E.; Milani, B. Palladium Alkyl Complexes with a Formazanate Ligand: Synthesis, Structure and Reactivity. *Dalton Trans.* **2018**, *47*, 14445−14451. (c) Milocco, F.; Demeshko, S.; Meyer, F.; Otten, E. Ferrate(II) Complexes with Redox-Active Formazanate Ligands. *Dalton Trans.* **2018**, *47*, 8817−8823.

(18) Chang, M.-C. *Formazanate as a Redox-Active, Structurally Versatile Ligand Platform: Zinc and Boron Chemistry*, PhD Thesis, University of Groningen, 2016.

(19) Pechmann, H. V. Ueber die Bildungsweisen der Formazylverbindungen. *Ber. Dtsch. Chem. Ges.* **1894**, *27*, 320−322.

(20) (a) Polumbrik, O. M.; Ryabokon, I. G.; Markovskii, L. N. Perfluorophenyl-containing verdazyl radicals. *Chem. Heterocycl. Compd.* **1980**, *16*, 882−885. (b) Hegarty, A. F.; Scott, F. L. The Synthesis of Formazans from Ortho-Substitued Arylidene Arylhydrazines. *J. Chem. Soc. C* **1967**, 2507−2508.

(21) Maar, R. R.; Barbon, S. M.; Sharma, N.; Groom, H.; Luyt, L. G.; Gilroy, J. B. Evaluation of Anisole-Substituted Boron Difluoride Formazanate Complexes for Fluorescence Cell Imaging. *Chem. - Eur. J.* **2015**, *21*, 15589−15599.

(22) Looney, A.; Han, R.; Gorrell, I. B.; Cornebise, M.; Yoon, K.; Parkin, G.; Rheingold, A. L. Monomeric Alkyl and Hydride Derivatives of Zinc Supported by Poly(pyrazoly)hydroborato Ligation: Synthetic, Structural, and Reactivity Studies. *Organometallics* **1995**, *14*, 274−288.

(23) Gilroy, J. B.; Patrick, B. O.; McDonald, R.; Hicks, R. G. Transition Metal Complexes of 3-Cyano- and 3-Nitroformazans. *Inorg. Chem.* **2008**, *47*, 1287−1294.

(24) (a) Chisholm, M. H.; Gallucci, J. C.; Phomphrai, K. Comparative Study of the Coordination Chemistry and Lactide Polymerization of Alkoxide and Amide Complexes of Zinc and Magnesium with a β-Diiminato Ligand Bearing Ether Substituents. *Inorg. Chem.* **2005**, *44*, 8004−8010. (b) Chen, H.-Y.; Huang, B.-H.; Lin, C.-C. A Highly Efficient Initiator for the Ring-Opening Polymerization of Lactides and ε-Caprolactone: A Kinetic Study. *Macromolecules* **2005**, *38*, 5400−5405.

(25) Dove, A. P.; Gibson, V. C.; Marshall, E. L.; White, A. J. P.; Williams, D. J. Magnesium and Zinc Complexes of a Potentially Tridentate β-Diketiminate Ligand. *Dalton Trans.* **2004**, 570−578.

(26) (a) Maar, R. R.; Barbon, S. M.; Sharma, N.; Groom, H.; Luyt, L. G.; Gilroy, J. B. Evaluation of Anisole-Substituted Boron Difluoride Formazanate Complexes for Fluorescence Cell Imaging. *Chem. - Eur. J.* **2015**, *21*, 15589−15599. (b) Maar, R. R.; Gilroy, J. B. Aggregation-Induced Emission Enhancement in Boron Difluoride Complexes of 3-Cyanoformazanates. *J. Mater. Chem. C* **2016**, *4*, 6478−6482.

(27) Laidler, K. J. *Chemical Kinetics*; 2nd ed.; 1965.

(28) Falivene, L.; Cao, Z.; Petta, A.; Serra, L.; Poater, A.; Oliva, R.; Scarano, V.; Cavallo, L. Towards the Online Computer-Aided Design of Catalytic Pockets. *Nat. Chem.* **2019**, *11*, 872−879.

https://dx.doi.org/10.1021/acs.organomet.0c00720
Organometallics 2021, 40, 63−71